Slow-fast dynamics of a time-delayed electro-optic oscillator

Lionel Weicker and Thomas Erneux
Université Libre de Bruxelles,
Optique Nonlinéaire Théorique,
Campus Plaine, C.P. 231,
1050 Bruxelles, Belgium

Otti D'Huys and Jan Danckaert
Applied Physics Research Group (APHY),
Vrije Universiteit Brussel,
1050 Brussel, Belgium

Maxime Jacquot, Yanne Chembo and Laurent Larger
Department of Optics,
UMR CNRS FEMTO-ST 6174,
University of Franche-Comté,
16 Route de Gray,
25030 Besançon Cedex, France

Abstract

Square-wave oscillations exhibiting different plateau lengths have been observed experimentally by investigating an electro-optic oscillator. In [20], we analyzed the model delay-differential equations and determined an asymptotic approximation of the two plateaus. In this paper, we concentrate on the fast transition layers between plateaus and show how they contribute to the total period. We also investigate the bifurcation diagram of all possible stable solutions. We show that the square-waves emerge from the first Hopf bifurcation of the basic steady state and that they may coexist with stable low-frequency periodic oscillations for the same value of the control parameter.

1 Introduction

Relaxation oscillations with alternate fast and slow phases appear in several areas of science from electronics to neural modelling. They are described mathematically as the solution of two or more nonlinear ordinary differential equations that exhibit different time scales. Over the years, reliable asymptotic

techniques such as the method of matched asymptotic expansions [2, 3] have been developed and successfully used to determine analytical expressions of physical interest (amplitude and period). The van der Pol equation in the large damping case is the reference problem for the analysis of relaxation oscillations [1, 2, 3] but other problems have emerged in the field of chemical and biological oscillations [4]-[6].

Analytical studies of relaxation oscillations that are solution of delay differential equations (DDEs) are however much rare. A notable exception is the analysis of a model for hematological stem cell regulation by Fowler and Mackey [7, 8]. The method of matched asymptotic expansions is difficult to implement for DDEs because we often need to anticipate the response of both the state and delayed variables. Much of the mathematical work that has been done [9]-[12] is concerned with scalar nonlinear DDEs of the form

$$\varepsilon x' = -x + f(x(t-1), \lambda). \tag{1}$$

where x' denotes the derivative of x with respect to the dimensionless time s ($s \equiv t/t_D$ where t is the real time and t_D is the delay of the feedback). $f(x, \lambda)$ is a nonlinear function of x and λ is a control parameter. $\varepsilon \equiv t_0/t_D > 0$ where t_0 is the linear decay time of x in the absence of feedback. Eq. (1) arises in a variety of applications, for example, physiological control systems [13], the transmission of light through a ring cavity [14]-[16], and population biology [17]. Under particular conditions on $f(x, \lambda)$ Eq. (1) may exhibit nearly 2-periodic square-wave oscillations provided ε is sufficiently small (see Figure 1). More precisely, these oscillations consist of sharp transition layers of size proportional to ε connecting plateaus that are close to the Period 2 fixed points of the map

$$x_n = f(x_{n-1}, \lambda) \tag{2}$$

where $x_n \equiv x(t)$ and $x_{n-1} \equiv x(t-1)$. The Period 2 fixed points of the map provide excellent approximations of the extrema of the oscillations. The description of the fast transition layers and the determination of the correction to the period is however much more delicate. Significant contributions to the asymptotic relations between the solutions of the map (2) and the solutions of the DDE (1) have been made by Chow and Mallet-Paret [9], Mallet-Paret and Nussbaum [10], Chow et al. [11] and Hale and Huang [12]. In particular, the Hopf bifurcation to the 2-periodic square-wave solutions has been carefully analyzed. As the bifurcation parameter deviates from its Hopf bifurcation value, the oscillations quickly change their shape from sinusoidal to square-waves [18].

Does Eq. (1) exhibit other type of square-wave oscillations? An analysis of the possible Hopf bifurcation points of Eq. (1) indicates that nearly 1-periodic square-wave solution are possible but are unstable because they emerge from an unstable steady state [18]. Moreover, transient asymmetric square waves exhibiting different plateau lengths can be initiated by choosing particular initial conditions but they disappear at finite time [19].

In [20], we addressed the question whether stable periodic square-wave oscillations exhibiting different plateau lengths (called duty cycles) are possible

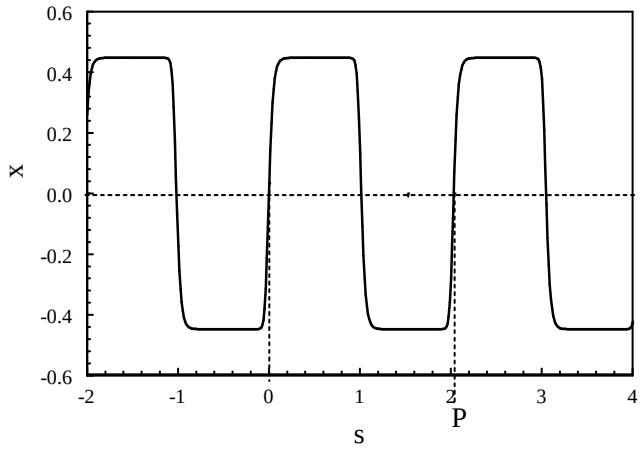

Figure 1: Nearly 2-periodic square-wave solution of Eq. (1) with $f(x,\lambda) = -\lambda x + x^3$. The values of the parameters are $\varepsilon = 0.02$ and $\lambda = 1.2$. The two plateaus are close to the period 2 fixed points of the map (2) given by $x_\pm = \pm\sqrt{\lambda - 1} = 0.45$. The period $P = 2 + O(\varepsilon)$ is slightly larger than 2 because of the time needed for the fast transition layers.

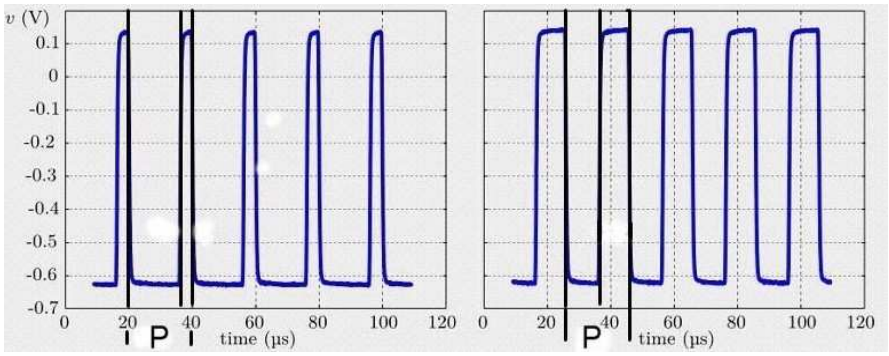

Figure 2: Experimental square-wave oscillations. By gradually changing the feedback phase Φ, the plateau lengths can be tuned but the total period $P \simeq t_D = 20\ \mu s$ remains fixed.

for problems modeled by second order DDEs. The question has been raised by experiments performed on electro-optic oscillators (EOOs) which are modeled mathematically in terms of second order DDEs [21, 22]. An EOOs typically incorporate a nonlinear (intensity) modulator, an optical-fiber delay line, and an optical detector in a closed-loop resonating configuration. This hybrid microwave source is capable of generating, within the same optoelectronic cavity, either an ultra-low-jitter (low phase-noise) single tone microwave oscillation, as used in radar applications [23, 24], or a broadband chaotic carrier typically intended for physical data encryption in high bit rate optical communications [25]. For a specific range of values of the parameters, periodic square-wave oscillations (see Figure 2) were found exhibiting a period P close to one delay t_D as well as different plateau lengths. It motivated an asymptotic analysis of the EOO equations in the limit of large delays. We obtained a good approximation of the plateaus and we were able to explain how their respective lengths depend on the control parameters [20].

In this paper, we concentrate on three different issues that were omitted in [20]. We first analyze the fast transition layers and show how they contribute to the total period. Second, we numerically investigate the bifurcation diagram of the square-wave oscillations and show how they emerge from a particular Hopf bifurcation. Third, we numerically found another stable time-periodic solution exhibiting a low frequency that may coexist with the square-wave solution. The plan of the paper is as follows. In Section 2, we introduce the EOO equations and propose a complete asymptotic description of the square-wave oscillations. In Subsection 2.1, the approximation of the slowly-varying plateaus is described in more detail than in [20]. The two fast transition layers are examined in Subsection 2.2. We show that they are described by the same equation which we analyze. In Section 3, we numerically investigate the bifurcation diagram of the stable solutions using two different methods. The main results are summarized in Section 4.

2 Asymptotic analysis

In dimensional form, the evolution equation for a EOO are (Eqs. (35) and (36) in [21] or Eqs. (3) and (4) in [20])

$$\begin{aligned} y' &= x, && (3)\\ \varepsilon x' &= -x - \delta y + \beta \left[\cos^2\left(x(s-1)+\Phi\right) - \cos^2(\Phi)\right], && (4) \end{aligned}$$

where prime means differentiation with respect to s and s is time measured in units of the delay. The parameters ε, δ, and Φ are fixed and given by [20]

$$\varepsilon = 10^{-3},\ \delta = 8.43 \times 10^{-3},\ \text{and } \Phi = -\frac{\pi}{4} + 0.1 \simeq -0.69. \qquad (5)$$

The feedback amplitude β is our bifurcation parameter.

Eqs. (3) and (4) admit nearly 1-periodic square-wave oscillations exhibiting different plateau lengths (see Figure 3). The slow/fast time behavior of the solution is due to the small value of ε. As we shall later demonstrate, the relatively

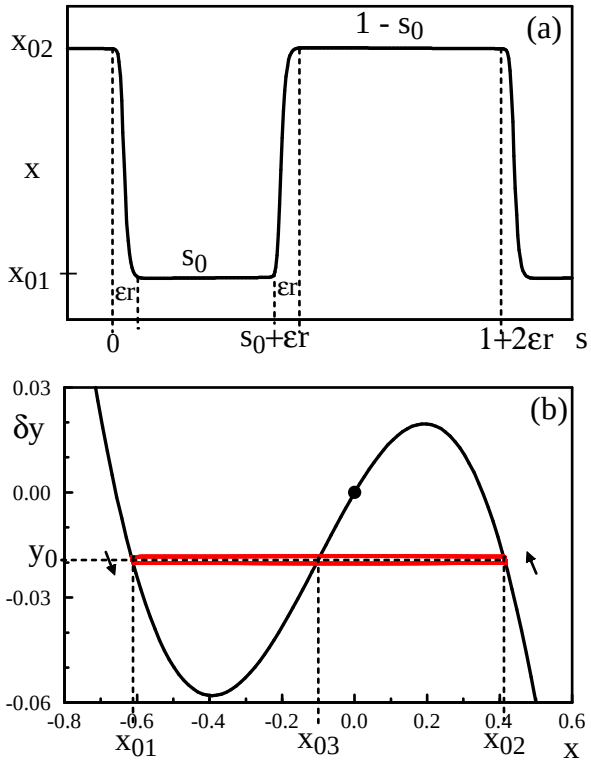

Figure 3: Colors on line. (a) Numerical square-wave solution of Eqs. (3) and (4) during one period. The values of the parameters are given by $\beta = 1.2$ and (5) except $\varepsilon = 5 \times 10^{-3}$ (this higher value of ε provides a better illustration of the fast transition layers). The two plateaus of the square-wave solution are of length s_0 and $1 - s_0$, respectively. The fast transition layers contributes to the total period by two corrections of size εr. (b) The periodic solution is shown in red in the phase plane $(x, \delta y)$. The S-shaped line is the function (11). The dot is the unique steady state $(x, y) = (0, 0)$. The values of $y_0 = -0.0192$, $x_{01} = -0.61$, $x_{03} = -0.1$, and $x_{02} = 0.41$ are determined in Subsection 2.1.

small change of y compared to x (see Figure 3b) is the result of the small value of δ. Furthermore, the asymmetry of the square-wave oscillations ($s_0 < 1/2$ in Figure 3a) is related to the deviation $\Phi + \pi/4$. Experimentally, we may explore different ranges of values of these parameters. In this paper, we shall keep δ and Φ fixed as given in (5) and consider different small values of ε whenever it becomes appropriate for our numerical illustrations or analysis.

We next propose to construct the square-wave solution in the limit $\varepsilon \to 0$. Specifically, we seek a P-periodic solution satisfying the condition

$$x(s - P) = x(s) \tag{6}$$

where the period P is given by

$$P = 1 + 2\varepsilon r \ (r = O(1)). \tag{7}$$

As shown in Figure 3a, the solution consists of two slowly varying plateaus connected by fast transition layers. We anticipate the analysis of the transition layers (see Subsection 2.2) by assuming that the contribution from these layers to the period P is the same (εr). We analyze the slow and fast parts of the solution, separately.

2.1 Slowly-varying plateaus

The leading approximation is obtained by setting $\varepsilon = 0$ in Eqs. (3)-(4). The reduced equations with (6) and (7) are

$$\begin{aligned} y' &= x, & (8)\\ 0 &= -x - \delta y + \beta \left[\cos^2(x + \Phi) - \cos^2(\Phi)\right] & (9)\\ x(s-1) &= x(s) & (10) \end{aligned}$$

From Eq. (9), we determine $y = y(x)$ as

$$y = \frac{1}{\delta}\left\{-x + \beta\left[\cos^2(x + \Phi) - \cos^2(\Phi)\right]\right\}. \tag{11}$$

The function (11) is represented in Figure 3b and exhibits three branches provided $\beta > 1$. The evolution of x and y along the left and right branches corresponds to the evolution along the plateaus of the square-wave periodic solution. They can be determined by inserting (11) into the left hand side of Eq. (8) and by solving the resulting first order equation for x. However, this solution is complicated and we may find simple analytical expressions by taking advantage of the small value of δ. Specifically, we seek a perturbation solution of Eqs. (8) and (9) of the form

$$\begin{aligned} y &= \delta^{-1} y_0(s) + y_{1j}(s) + ... & (12)\\ x &= x_{0j}(s) + \delta x_{1j}(s) + ... & (13) \end{aligned}$$

where $j = 1$ or 2 refer to the time domains $0 < s < s_0$ and $s_0 < s < 1$, respectively. (see Figure 4).

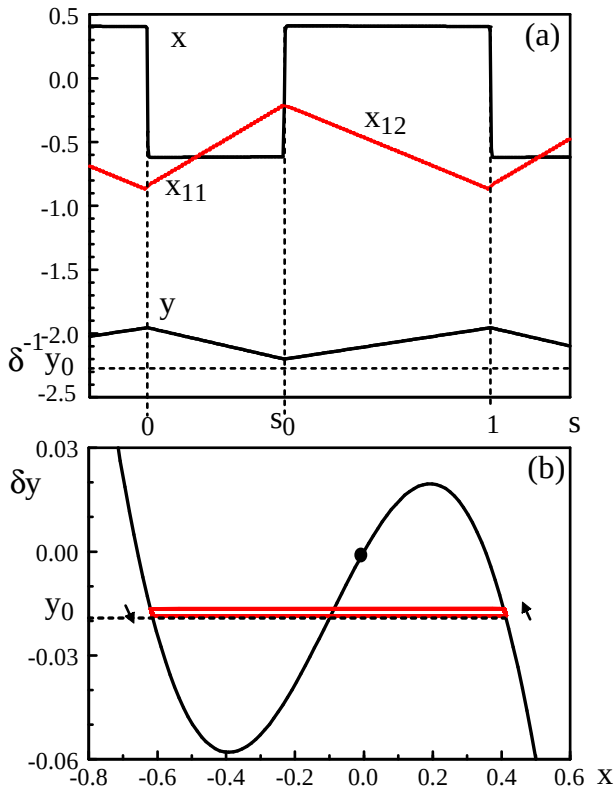

Figure 4: Colors on line. Numerical square-wave solution of Eqs. (3) and (4) during one period. The values of the parameters are the same as for Figure 3a except that $\varepsilon = 2\times10^{-4}$ is much smaller. (a) $x(s)$ exhibits sharp jumps at times $s = 0$, $s = s_0$, and $s = 1$ while y remains continuous at those points. We also determine $x_{1j} \simeq (x - x_{0j})/\delta$ (red) and note that x_{11} and x_{12} are continuous at times 0, s_0, 1. (b) The square-wave periodic solution is shown in the phase-plane $(x, \delta y)$ (red). Comparing with Figure 3b, we note that $\delta y = y_0$ is now located slightly below the closed orbit.

Inserting (12) and (13) into Eqs. (8)-(9) and equating to zero the coefficients of each power of δ leads to a sequence of problems for the unknowns functions y_0, y_{1j}, x_{0j},and x_{1j}.The leading order problem is $O(1)$ and is given by

$$\begin{aligned} y_0' &= 0, && (14)\\ -x_{0j} - y_0 + \beta\left[\cos^2(x_{0j}+\Phi) - \cos^2(\Phi)\right] &= 0. && (15) \end{aligned}$$

Eq (14) implies that y_0 is a constant. We already know that for a finite range of values of y_0, Eq. (15) admits more than one root (see Figure 3b). The solutions corresponding to the left and right branches are denoted by $x_{01} < 0$ and $x_{02} > 0$, respectively. We don't know the values of y_0 and analyze the $O(\delta)$ problem for $y_{1j}(s)$ and $x_{1j}(s)$. It is given by

$$\begin{aligned} 0 &\le s < s_0 && \\ y_{11}' &= x_{01}, && (16)\\ -x_{11} - y_{11} - 2\beta\sin(2x_{01}+2\Phi)x_{11} &= 0, && (17)\\ s_0 &\le s < 1 && \\ y_{12}' &= x_{02}, && (18)\\ -x_{12} - y_{12} - 2\beta\sin(2x_{02}+2\Phi)x_{12} &= 0. && (19) \end{aligned}$$

Figure 4 suggests the following initial conditions for y_{11} and y_{12}

$$y_{11}(0) = y_{1M} \text{ and } y_{12}(s_0) = y_{1m} \tag{20}$$

where y_{1M} and y_{1m} corresponds to the maximum of y_{11} and the minimum of y_{12}, respectively. The solution of Eqs. (16)-(20) then is

$$\begin{aligned} y_{11} &= y_{1M} + x_{01}s, && (21)\\ y_{12} &= y_{1m} + x_{02}(s - s_0), && (22)\\ x_{11} &= -\frac{y_{11}}{1 + 2\beta\sin(2x_{01}+2\Phi)}, && (23)\\ x_{12} &= -\frac{y_{12}}{1 + 2\beta\sin(2x_{02}+2\Phi)}. && (24) \end{aligned}$$

continuity of y_{11} and y_{12} at times $s = s_0$ and 1 leads to the conditions

$$\begin{aligned} y_{1M} + x_{01}s_0 &= y_{1m}, && (25)\\ y_{1m} + x_{02}(1 - s_0) &= y_{1M} && (26) \end{aligned}$$

which are two equations for $y_{1M} - y_{1m}$. A solution of Eqs. (25) and (26) is possible only if

$$x_{01}s_0 + x_{02}(1 - s_0) = 0. \tag{27}$$

As for y_{11} and y_{12}, we next assume that the corrections x_{11} and x_{12} are equal at $s = s_0$ and $s = 1$ (see Figure 4a). From (23) and (24), we then obtain the condition

$$\sin(2x_{01} + 2\Phi) = \sin(2x_{02} + 2\Phi), \tag{28}$$

or equivalently,

$$\cos(x_{01} + x_{02} + 2\Phi)\sin(x_{01} - x_{02}) = 0. \tag{29}$$

Eq. (29) admits multiple solutions. We specifically look for a solution of Eq. (29) which satisfies the perfect square-wave condition $x_{01} = -x_{02}$ if $\Phi = -\pi/4$. This solution is given by

$$x_{01} + x_{02} + 2\Phi = -\pi/2. \tag{30}$$

Using (15), (30) allows to determine y_0, x_{01} and x_{02}. Substracting Eq. (15) with x_{01} and Eq. (15) with x_{02} gives

$$-(x_{01} - x_{02}) - \beta\sin(x_{01} + x_{02} + 2\Phi)\sin(x_{01} - x_{02}) = 0 \tag{31}$$

Using (30) then allows to eliminate x_{02} in Eq. (31). We find

$$-(2x_{01} + 2\Phi + \pi/2) + \beta\sin(2x_{01} + 2\Phi + \pi/2) = 0. \tag{32}$$

Eq. (32) provides the solution for $x_{01} = x_{01}(\beta)$ in the implicit form

$$\beta = \frac{2x_{01} + 2\Phi + \pi/2}{\sin(2x_{01} + 2\Phi + \pi/2)}. \tag{33}$$

We obtain x_{02} and s_0 by using (30) and (27)

$$x_{02} = -\pi/2 - 2\Phi - x_{01}, \tag{34}$$

$$s_0 = \frac{x_{02}}{x_{02} - x_{01}}. \tag{35}$$

In Figure 5, we compare our approximations with the numerical solution obtained for $\beta = 1.2$? The expression for y_0 as well as for x_{03}, defined as the third root of Eq. (15), are documented in the appendix. In Section 3, we numerically analyze the bifurcation diagram of the possible stable solutions and show that the square-wave oscillations emerge from a Hopf bifurcation.

2.2 The fast transition layers

The plateaus of the square-wave are connected by fast transition layers on time intervals proportional to ε. See Figure 3a.

2.2.1 Jump down at $s = 0$

We first consider the fast transition layer at $s = 0$ and introduce the inner variable $\zeta_1 \equiv s\varepsilon^{-1}$. The leading order transition layer equations for $y = Y_1(\zeta_1)$ and $x = X_1(\zeta_1)$ are then given by

$$\frac{dY_1}{d\zeta_1} = 0, \tag{36}$$

$$\frac{dX_1}{d\zeta_1} = -X_1 - \delta Y_1 + \frac{\beta}{2}\left[\cos(2X_1(\zeta_1 + 2r) + 2\Phi) - \cos(2\Phi)\right] \tag{37}$$

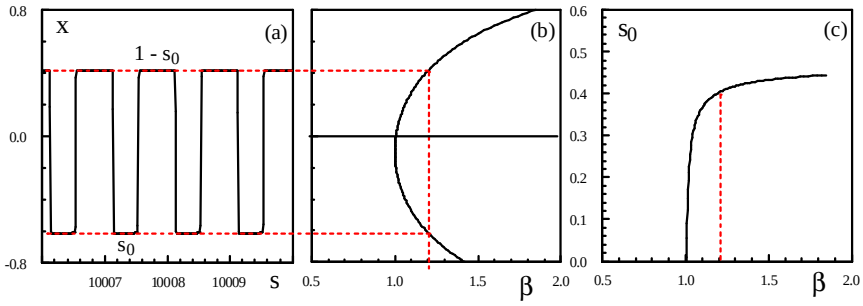

Figure 5: Colors on line. Analytical bifurcation diagram of the square-waves. (a) The numerically computed square-wave is shown for $\beta = 1.2$ and the values of the parameters listed in (5). (b) Its extrema are in good agreement with the analytical predictions obtained from the parametric solution (33) - (35) (with x_{01} as the parameter). (c) The plateau lengths are s_0 and $1 - s_0$, respectively, and the figure shows s_0.

where we have used the periodicity condition

$$x(s-1) = x(s - P + 2\varepsilon r) = x(s + 2\varepsilon r) = X_1(\zeta_1 + 2r). \tag{38}$$

Eq. (36) implies that Y_1 is a constant. It needs to match the constant determined in our analysis of the slowly varying plateaus i.e., $Y_1 = y_0\delta^{-1}$ Using the expression of y_0 given by (66), Eq. (37) can be rewritten as

$$\frac{dX_1}{d\zeta_1} = -X_1 - \Phi - \frac{\pi}{4} + \frac{\beta}{2}\sin(2X_1(\zeta_1 + 2r) + 2\Phi + \frac{\pi}{2}). \tag{39}$$

This equation can be reformulated in a simpler form by introducing the deviation $z_1 \equiv X_1 - x_{03} = X_1 + \Phi + \frac{\pi}{4}$. From Eq. (39), we obtain

$$\frac{dz_1}{d\zeta_1} = -z_1 + \frac{\beta}{2}\sin(2z_1(\zeta_1 + 2r)). \tag{40}$$

The boundary conditions for the jump down transition are $X_1(-\infty) = x_{02}$ and $X_1(\infty) = x_{01}$. In terms of z_1, they take the simpler form

$$z_1(-\infty) = a \text{ and } z_1(\infty) = -a \tag{41}$$

where

$$a \equiv x_{02} - x_{03} > 0. \tag{42}$$

2.2.2 Jump up at $s = s_0 + \varepsilon r$

We next consider the transition layer near $s = s_0 + \varepsilon r$ and introduce the inner variable $\zeta_2 \equiv (s - s_0 - \varepsilon r)\varepsilon^{-1}$. The leading order transition layer equations for

$y = Y_2(\zeta_2)$ and $x = X_2(\zeta_2)$ are given by

$$\frac{dY_2}{d\zeta_2} = 0, \tag{43}$$

$$\frac{dX_2}{d\zeta_2}(\zeta_2 + \frac{s_0+\varepsilon r}{\varepsilon}) = -X_2(\zeta_2 + \frac{s_0+\varepsilon r}{\varepsilon}) - \delta Y_2(\zeta_2 + \frac{s_0+\varepsilon r}{\varepsilon}) + \frac{\beta}{2}\left[\begin{array}{c}\cos(2X_2(\zeta_2 + \frac{s_0+\varepsilon r}{\varepsilon} + 2r) + 2\Phi) \\ -\cos(2\Phi)\end{array}\right]. \tag{44}$$

where we have used the periodicity condition

$$x(s-1) = x(s-P+2\varepsilon r) = x(s+2\varepsilon r) = X_2(\zeta_2 + \frac{s_0+\varepsilon r}{\varepsilon} + 2r). \tag{45}$$

The constant solution for Y_2 is again matching the value obtained from the analysis of slowly varying plateaus i.e., $Y_2 = y_0\delta^{-1}$ Using the expression of y_0 given by (66), Eq. (44) simplifies as

$$\frac{dX_2}{d\zeta_2}(\zeta_2 + \frac{s_0+\varepsilon r}{\varepsilon}) = -X_2(\zeta_2 + \frac{s_0+\varepsilon r}{\varepsilon}) - \Phi - \frac{\pi}{4} + \frac{\beta}{2}\sin(2X_2(\zeta_2 + \frac{s_0+\varepsilon r}{\varepsilon} + 2r) + 2\Phi + \frac{\pi}{2}). \tag{46}$$

Introducing the deviation $z_2 \equiv X_2 - x_{03} = X_2 + \Phi + \frac{\pi}{4}$, Eq. (46) becomes

$$\frac{dz_2}{d\zeta_2}(\zeta_2 + \frac{s_0+\varepsilon r}{\varepsilon}) = -z_2(\zeta_2 + \frac{s_0+\varepsilon r}{\varepsilon}) + \frac{\beta}{2}\sin(2z_2(\zeta_2 + \frac{s_0+\varepsilon r}{\varepsilon} + 2r). \tag{47}$$

We next note the following relations between the two inner variables

$$\zeta_2 = \zeta_1 - \frac{s_0+\varepsilon r}{\varepsilon}. \tag{48}$$

Inserting (48) into Eq. (47), we formulate an equation for $z_2(\zeta_1)$ of the form

$$\frac{dz_2}{d\zeta_1}(\zeta_1) = -z_2(\zeta_1) + \frac{\beta}{2}\sin(2z_2(\zeta_1 + 2r)). \tag{49}$$

The boundary conditions for the second transition layer now are

$$z_2(-\infty) = -a \text{ and } z_2(\infty) = a \tag{50}$$

where a is defined by (42). We realize that Eqs. (49) and (50) are the same as Eqs. (40) and (41) except that the boundary conditions have been interchanged. This implies that the solution of Eqs. (49) and (50) is related to the solution of Eqs. (40) and (41) by

$$z_2(\zeta_1) = -z_1(\zeta_1). \tag{51}$$

In conclusion, we found the same delay differential equation for the two fast transition layers. It is given by

$$\frac{dz}{d\zeta} = -z + \frac{\beta}{2}\sin(2z(\zeta + 2r)), \tag{52}$$

$$z(-\infty) = a \text{ and } z(\infty) = -a \tag{53}$$

where we have omitted the subscript 1 for z_1 and ζ_1 We next proceed as in [9]. We note that by rescaling time ζ as $\xi \equiv -\zeta/2r$, Eq. (52) can be rewritten as a DDE with delay 1 and parameter r

$$\begin{aligned} \frac{dz}{d\xi} &= 2r\left[z - \frac{\beta}{2}\sin(2z(\xi-1))\right] && (54) \\ z(-\infty) &= a \text{ and } z(\infty) = -a. && (55) \end{aligned}$$

$z = \pm a$ are both critical points of Eq. (54). This means that we are looking for a heteroclinic orbit for some value of r, that is, a trajectory joining these critical points as $\xi \to \pm\infty$. The delay parameter r is unknown a priory, and must be determined as part of the solution. We cannot solve the problem analytically for arbitrary β (it is a nonlinear DDE).

2.2.3 Correction to the period

In this subsection, we solve Eq. (54) and (55) for β close to 1. Our objective is to demonstrate that there is indeed a unique value of r such that Eq. (54) and (55) admits a solution. To this end, we introduce a small parameter μ defined by .

$$\mu \equiv \sqrt{(\beta-1)/b} \tag{56}$$

where $b = \pm 1$ if $\beta \gtrless 1$. We then expand the solution z and parameter r in power series of μ

$$\begin{aligned} z &= \mu Z_1(\nu) + \mu^2 Z_2(\nu) + ... && (57) \\ r &= r_0 + \mu r_1 + ... && (58) \end{aligned}$$

where $\nu \equiv \mu\xi$. The motivation for introducing (56) comes from the fact that $a \equiv x_{02} - x_{03} = \sqrt{\frac{3}{2}(\beta-1)}$, in first approximation as $\beta \to 1$, which implies that the amplitude of the solution scales like $\sqrt{\beta-1}$. After introducing (56)-(58) into (52), we equate to zero the coefficients of each power of μ. The leading order problem is $O(\mu)$ and is given by

$$(1 - 2r_0)\frac{dZ_1}{d\nu} = 0 \tag{59}$$

In order to have a non constant solution for z_1 we requires that $r_0 = 1/2$. The next problem is $O(\mu^2)$ and is given by

$$-\frac{1}{2}\frac{d^2Z_1}{d\nu^2} + \frac{2}{3}Z_1^3 - bZ_1 + 2r_1\frac{dZ_1}{d\nu} = 0 \tag{60}$$

with the boundary conditions

$$Z_1(-\infty) = \sqrt{3b/2} \text{ and } Z_1(\infty) = -\sqrt{3b/2}. \tag{61}$$

We choose $b = 1$ and note that the damped Hamiltonian equation (60) has a unique solution $z_1 = -\sqrt{3/2}\tanh(\nu)$ if $r_1 = 0$. We conclude that we have found an analytical expression for the transition layer solution provided

$$\beta > 1 \text{ and } r = \frac{1}{2} + O((\beta - 1)). \tag{62}$$

We have determined numerically the period of the square-wave oscillations with a high precision. The values of δ and Φ are documented in (5), $\varepsilon = 5 \times 10^{-2}$, and $\beta = 1.2$. We find $P \simeq 1.047$. From (7), we then compute $2\varepsilon r = 4.710^{-2}$ which implies $r = 0.47$. The numerical value of r is close to the analytical value $r = 0.5$ given in (62).

3 Numerical bifurcation diagrams

We consider β as our bifurcation parameter. All other parameters are documented in (5). A linear stability analysis of the steady state $(x, y) = (0, 0)$ allows us to determine the primary Hopf bifurcation points and Hopf frequencies. They satisfy the following equations

$$\tan(\sigma) = -\left[\frac{\varepsilon\sigma^2 - \delta}{\sigma}\right], \tag{63}$$

$$\beta = -\frac{1}{\sin(2\Phi)\cos(\sigma)}. \tag{64}$$

The first Hopf bifurcation is located at $\beta = \beta_1 \simeq 1.020$ and exhibits a frequency close to 2π ($\sigma_1 = 6.28$). Using a continuation method, we find a 1-periodic branch of periodic solutions that connects the asymmetric square-waves (see Figure 6a). More precisely, the Hopf bifurcation branch is first subcritical and unstable and then folds back to a branch of stable square-wave oscillations. There are many more Hopf bifurcation points as we further increase β from β_1. Using different initial conditions, we have integrated numerically Eqs. (3) and (4) , and found another branch of stable periodic solutions. By contrast to the square-wave oscillations, the new oscillations exhibit a low frequency. We have found that it emerges from the primary Hopf bifurcation point $\beta = \beta_2 \simeq 1.025$ as an unstable branch (as expected since this bifurcation is from an unstable steady state) and then stabilizes as $\beta \geq 1.029$. The frequency at the Hopf bifurcation point is $\sigma_2 = 0.09$ meaning a period $P = 69.81$ (numerically, we found $P = 69.12$ see Figure 7b)

The bifurcation diagrams shown in Figure 6 illustrate the results of our simulations. The first Hopf bifurcation leads to the asymmetric square-wave oscillations that we investigated analytically in Section 2. Specifically, the extrema of x as a function of β are given by (33) and (35) where $x_{01} \geq -\pi/4 - \Phi$ (full red line in Figure 6a and full black line in Figure 6b) .In Figure 6b, the square dots are the solutions obtained numerically from simulating the full equations (3) and (4). For each point, the initial conditions were $x = -1$ ($-1 \leq s < -1/3$),

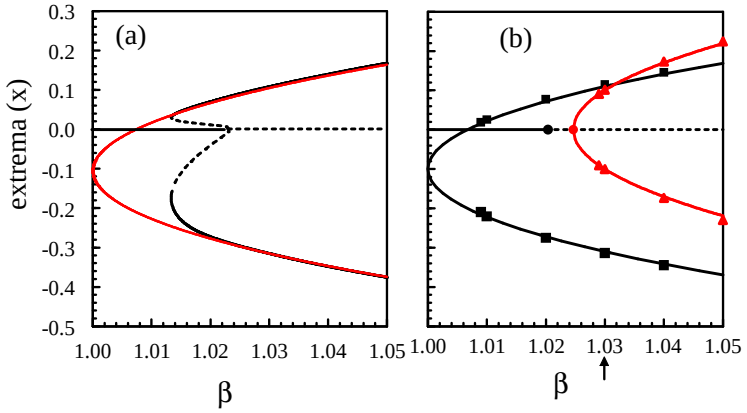

Figure 6: Colors on line. (a) Bifurcation diagram of the 1-periodic square-waves obtained by a continuation method. The values of the parameters are listed in (5) except $\Phi = -0.68$ and $\varepsilon = 5.5 \times 10^{-3}$). Full and broken lines correspond to stable and unstable solutions, respectively. The red parabolic line emerging at $(\beta, x) = (1, -0.1)$ is the analytical approximation given by (33) and (34). (b) Bifurcation diagram of the 1-periodic square-waves obtained by numerical integration. The values of the parameters are listed in (5). The full black line represents the analytical approximation given by (33) and (34). The square dots and the red triangles denote stable periodic solutions obtained by integrating Eqs. (3) and (4). The squares and the triangles correspond to square-wave and low frequency periodic solutions, respectively. The change of stability of the zero solution occurs at $\beta = \beta_1 \simeq 1.020$ and corresponds to a Hopf bifurcation to the 1-periodic square-wave oscillations. The red parabolic lines are curve fitting lines given by $x = \pm 1.3742\sqrt{\beta - \beta_2}$ where $\beta_2 = 1.025$ is the primary Hopf bifurcation point leading to the low frequency oscillations and obtained from the linearized theory. In Figure 7, we show the two stable solutions coexisting for $\beta = 1.03$ (this value of β is indicated by an arrow).

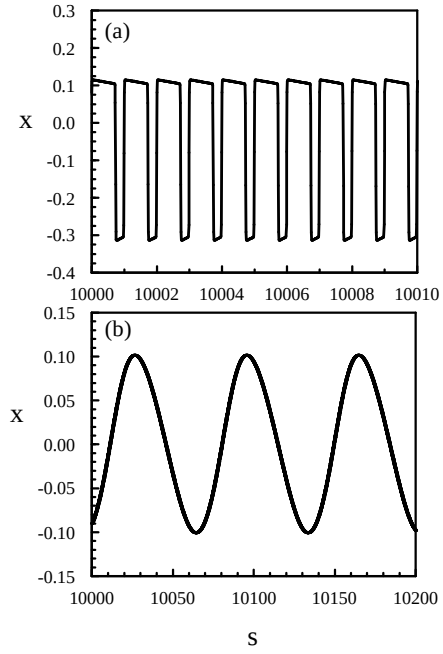

Figure 7: Coexistence of two different stable periodic solutions. The values of the parameters are documented in (5) and $\beta = 1.03$. (a) The 1 -periodic square-wave is obtained using $x = -1$ $(-1 < s \leq -2/3)$, $x = 1$ $(-2/3 < s \leq 0)$, .and $y(0) = 0$. (b) The low- frequency oscillations are found using $x = \cos(0.33s)$ $(-1 < s \leq 0)$ and $y(0) = 0$.

$x = 1$ $(-1/3 \leq s < 0)$, and $y(0) = 0$. The long time solution was then analyzed when $s > 10000$. For $\beta < 1.009$, the system jumps to the zero solution. The stability of the zero solution was also tested by using the initial conditions $x = 0$ $(-1 \leq s < -1/3)$, $x = 10^{-3}$ $(-1/3 \leq s < 0)$, and $y(0) = 0$. The long time solution was again analyzed when $s > 10000$. For $\beta = 1.020$, $x = 0$ is stable. For $\beta = 1.021$, $x = 0$ is unstable and the the system jumps to the 1-periodic asymmetric square-wave. In addition to the 1-periodic square-wave solution, a stable low frequency periodic solution was determined as soon as $\beta \geq 1.029$. The initial conditions were $x = 0.1\cos(0.33s)$ $(-1 \leq s < 0)$ and $y(0) = 0$. At $\beta = 1.029$, the frequency of the oscillations is $\sigma = 0.095$ which is close to the Hopf frequency σ_2. The parabolic lines given by $x = \pm 1.3742\sqrt{\beta - \beta_2}$ are curve fitting curves that strongly suggest that the unstable branch of periodic solutions emerging at $\beta = \beta_2 = 1.025$ stabilizes as soon as $\beta \geq 1.029$. Similar responses (square-wave or low-frequency oscillations) have been found previously [21] but not for the same values of the bifurcation parameter. Here, the two distinct regimes may coexist (see Figure 7).

4 Discussion

In this paper, we investigated several issues that were missing in [20]. First, we concentrate on the fast transition layers between the plateaus of the square-waves and showed how they contribute to the correction of the total period. Second, we show numerically that the square-wave oscillations are the result of a first Hopf bifurcation from the basic steady state. The bifurcation is subcritical and allows the coexistence of stable square-waves with a stable steady state. Experiments done on a EOO oscillator using quite different values of the parameters [22] suggest that the same mechanism could be responsible for the onset of asymmetric square-waves. There are many other primary Hopf bifurcation points but we found only one leading to stable oscillations. The new periodic solution exhibits a large period and smooth oscillations. An asymptotic description of this solution is also possible [21]. Both the square-wave and the large period oscillations are the result of the large delay. They are dominant attractors in our EOO problem and motivate the investigation of other second-order nonlinear DDEs experiencing a large delay.

Acknowledgements

We thank D.P. Rosin, D.J. Gauthier, and E. Schöll for fruitful discussions at the conference in Palma. We also thank the referees for valuable questions. T.E. and L.W. acknowledge the support of the F.N.R.S. (Belgium) and the Belgian F.R.I.A. for a PhD scholarship, respectively. This work benefited from the support of the Belgian Science Policy Office under Grant No IAP-7/35 "photonics@be". It was also supported by the European project PHOCUS (FP7 grant 240763). L.L. thanks the support of the *Institut Universitaire de France*

References

[1] C.M. Bender and S.A. Orszag, "Advanced Mathematical Methods for Scientists and Engineers", Mc Graw Hill, New York (1978)

[2] J. Kevorkian and J.D. Cole, "Perturbation Methods in Applied Mathematics", Appl. Math.l Sciences **34**, Springer, New York (1981); "Multiple Scale and Singular Perturbation Methods", Appl. Math. Sciences **114**, Springer, New York (1996)

[3] J. Grasman, "Asymptotic Methods of Relaxation Oscillations and Applications", Applied Mathematical Sciences **63** Springer New York (1987)

[4] A.C. Fowler, "Mathematical Models in the Applied Sciences", Cambridge Texts in Applied Mathematics, Cambridge University Press, Cambridge (1997)

[5] J. Keener and J. Sneyd, "Mathematical Physiology", Springer-Verlag, New York (1998)

[6] J.D. Murray, "Mathematical Biology I: An Introduction", Inter. Appl. Mathematics **17**, Springer, Berlin Third Edition (2002)

[7] A.C. Fowler and M.C. Mackey, Relaxation oscillations in a class of delay differential equations, SIAM J. Appl. Math. **63**, 299–323 (2002)

[8] A.C. Fowler, Asymptotic methods for delay equations, Journal of Engineering Mathematics **53**, 271–290 (2005)

[9] S.N. Chow, J. Mallet-Paret, Singularly pertubed delay differential equations, in "Coupled Nonlinear Oscillators", Proceedings of the Joint U.S. Army - Center for Nonlinear Studies Workshop, Los Alamos, New Mexico, pp. 7-12 (1983)

[10] J. Mallet-Paret, R.D. Nussbaum, Global continuation and asymptotic behavior for periodic solutions of a differential-delay equation, Ann. Mat. Pura Appl. **145**, 33-28.(1986)

[11] S.N. Chow, J.K. Hale, W. Huang, From sine waves to square waves in delay equations, Proc. Roy. Soc. Edinburgh Sect. A-Math. **120**, 223-229 (1992)

[12] J.K. Hale, W.Z. Huang, Period-doubling in singularly perturbed delay equations, J. Diff. Equ. **114**, 1-23 (1994); J.K. Hale, W.Z. Huang, Periodic solutions of singularly perturbed delay equations, Z. Angew. Math. Phys. **47**, 57-88 (1996)

[13] M.C. Mackey, L. Glass, Oscillation and chaos in physiological control-systems, Science **197**, 287-288 (1977).

[14] K. Ikeda, Multiple-valued stationary state and its instability of the transmitted light by a ring cavity system, Opt. Commun. **30,** 257-261 (1979)

[15] K. Ikeda, H. Daido, O. Akimoto, Optical turbulence - chaotic behavior of transmitted light from a ring cavity, Phys. Rev. Lett. **45**, 709-712 (1980).

[16] K. Ikeda, O. Akimoto, Successive bifurcations and dynamical multistability in a bistable optical-system a detailed study of the transition to chaos, Appl. Phys. B **28**, 170-171 (1982).

[17] W.S.C. Gurney, S.P. Blythe, and R.M. Nisbet, Nicholson's blowflies revisited, Nature **287**, 17-21 (1980)

[18] T. Erneux, L. Larger, M. W. Lee, J.-P.Goedgebuer, Ikeda Hopf bifurcation revisited, Physica D **194**, 49-64 (2004)

[19] T. Erneux, "Applied Delay Differential Equations", Springer 2009

[20] L. Weicker, T. Erneux, O. d'Huys, J. Danckaert, M. Jacquot, Y. Chembo, and L. Larger, Strongly asymmetric square-waves in a time delayed system, Phys. Review E **86**, 055201(R) (2012)

[21] M. Peil, M. Jacquot, Y. Kouomou Chembo, L. Larger, and T. Erneux, Routes to chaos and multiple time scale dynamics in broadband bandpass nonlinear delay electro-optic-oscillators, Phys. Rev. E **79**, 026208 (2009)

[22] D.P. Rosin, K.E. Callan, D.J. Gauthier, and E. Schöll, Pulse-train solutions and excitability in an optoelectronic oscillator, Eur. Phys. Lett. **96**, 34001 (2011)

[23] J. Lasri, P. Devgan, R. Tang, and P. Kumar, Self-starting optoelectronic oscillator for generating ultra-low-jitter high-rate (10GHz or higher) optical pulses, Optics Express **11**, 1430-1435 (2003); ibidem, Ultralow timing jitter 40-Gb/s clock recovery, IEEE Phot. Techn. Lett.16, 263-265 (2004)

[24] Y.K. Chembo, A. Hmima, P.A. Lacourt, L. Larger, J.M. Dudley, Generation of ultralow jitter optical pulses using optoelectronic oscillators with time-lens soliton-assisted compression, Journal of Lightwave and Technology **27**, 5160-5167, (2009)

[25] L. Larger and J.-P. Goedgebuer, Encryption using chaotic dynamics for optical telecommunications, C.R. de Physique **5**, 609-611 (2004)

[26] K. Engelborghs, T. Luzyanina, and D. Roose. Numerical bifurcation analysis of delay differential equations using DDE-BIFTOOL. ACM Transactions on Mathematical Software, 28(1):1–21 (2002)

5 Appendix

The plateaus of the square-wave are $x = x_{01} < 0$ and $x = x_{02} > 0$, in first approximation. They are defined as two roots of Eq. (15) for a fixed y_0. Figure 3b suggests that there is a third root. In this appendix, we determine this third root and formulate an expression for y_0.

Equations for x_{01} and x_{02} are given by Eqs. (30) and (32). From Eq. (32) we determine $\beta\cos(2x_{01}+2\Phi)$ as

$$\beta\cos(2x_{01}+2\Phi) = 2x_{01}+2\Phi+\frac{\pi}{2}. \tag{65}$$

From (15) with $j=1$, we formulate an expression for y_0 given by

$$y_0 = -x_{01}+\frac{\beta}{2}\cos(2x_{01}+2\Phi)-\frac{\beta}{2}\cos(2\Phi)$$

Using (65)

$$\begin{aligned} y_0 &= -x_{01}+\frac{1}{2}(2x_{01}+2\Phi+\frac{\pi}{2})-\frac{\beta}{2}\cos(2\Phi) \\ &= \Phi+\frac{\pi}{4}-\frac{\beta}{2}\cos(2\Phi). \end{aligned} \tag{66}$$

In order to find the third root of Eq. (15), we introduce (66) into Eq. (15) and obtain

$$\Phi + \frac{\pi}{4} = -x_{0j} + \frac{\beta}{2}\cos(2x_{0j} + 2\Phi). \tag{67}$$

This equation admits the solution

$$x_{03} = -(\Phi + \frac{\pi}{4}). \tag{68}$$

Using Eq. (30), we then obtain the relation

$$x_{01} + x_{02} = 2x_{03} \tag{69}$$

or equivalently,

$$x_{02} - x_{03} = x_{03} - x_{01}. \tag{70}$$

The two extreme roots are at equal distance from the central root x_{03}. This symmetry property has important consequences. In particular, the two fast transitions layers admit the same equation and they contribute in the same way to the correction of the period.